

# Chaos in dynamic atomic force microscopy

F Jamitzky<sup>1,2</sup>, M Stark<sup>3</sup>, W Bunk<sup>2</sup>, W M Heckl<sup>1,4</sup> and R W Stark<sup>1</sup>

<sup>1</sup> Center for Nanoscience (CeNS) and Ludwig-Maximilians-Universität, Department of Earth and Environmental Science, Crystallography, 80333 Munich, Germany

<sup>2</sup> Max-Planck-Institut für Extraterrestrische Physik, 85748 Garching, Germany

<sup>3</sup> Ecole Polytechnique Fédérale de Lausanne, Laboratory of Ultrafast Spectroscopy, Institut des Sciences et Ingénierie Chimiques, FSB-BSP, CH-1015 Lausanne-Dorigny, Switzerland

<sup>4</sup> Deutsches Museum, Museumsinsel 1, 80538 Munich, Germany

E-mail: [fxj@mpe.mpg.de](mailto:fxj@mpe.mpg.de) and [stark@nanomanipulation.de](mailto:stark@nanomanipulation.de)

Received 22 August 2005

Published 10 March 2006

Online at [stacks.iop.org/Nano/17/S213](http://stacks.iop.org/Nano/17/S213)

## Abstract

In tapping mode atomic force microscopy (AFM) the highly nonlinear tip–sample interaction gives rise to a complicated dynamics of the microcantilever. Apart from the well-known bistability under typical imaging conditions the system exhibits a complex dynamics at small average tip–sample distances, which are typical operation conditions for mechanical dynamic nanomanipulation. In order to investigate the dynamics at small average tip sample gaps experimental time series data are analysed employing nonlinear analysis tools and spectral analysis. The correlation dimension is computed together with a bifurcation diagram. By using statistical correlation measures such as the Kullback–Leibler distance, cross-correlation and mutual information the dataset can be segmented into different regimes. The analysis reveals period-3, period-2 and period-4 behaviour, as well as a weakly chaotic regime.

## 1. Introduction

Atomic force microscopy (AFM) is widely used for surface inspection with nanometre resolution in engineering applications as well as in fundamental research. In particular, dynamic AFM measurement methods such as tapping mode or noncontact mode are common imaging modes. Despite the widespread application of dynamic AFM the nonlinear dynamics of the vibrating force sensor is still a topic of intense research [1]. The force sensing microcantilever is forced to oscillation amplitudes of several tens of nanometres in the so-called ‘tapping mode’ of operation, which is also referred to as ‘amplitude modulation AFM’. Usually, the driving frequency is adjusted to or very close to the fundamental resonant frequency of the free cantilever and the driving amplitude is set to a constant value. Typical resonant frequencies are in the range from a few kilohertz to some megahertz. When the specimen is brought close to the oscillating probe, the amplitude is reduced due to the interaction forces between the tip and the surface.

The amplitude ratio  $A/A_0$  of the actual oscillation amplitude  $A$  to the oscillation amplitude of the free cantilever

$A_0$  is used for feedback. Employing a PD controller with the set-point  $A_s$  the tracking error  $e = A_s - A/A_0$  is minimized by controlling the  $z$ -position of the sample and thus keeping the average tip–sample gap constant. The specimen can be thought of as a hard barrier limiting the oscillatory amplitude, which results in a strongly nonlinear system dynamics. The external forcing together with the nonlinearity leads to the coexistence of a non-touching (also known as ‘attractive’ or ‘low amplitude’) system state with a touching (‘repulsive’ or ‘high amplitude’) solution under standard imaging conditions. The dynamics and the consequences of this bistability are amongst the most extensively investigated features of the nonlinear dynamics in tapping mode AFM [1].

In addition to the bistable system response, theoretical studies have shown that the strongly nonlinear interaction between tip and sample also can lead to a complex dynamics although the system is usually well behaved for typical parameters as they occur under typical imaging conditions [2–6]. From numerical simulations, Ashhab *et al* [7, 8] conclude that chaos can exist in dynamic force microscopy depending on the damping, excitation and average tip–sample distance. They suggest employing a state feedback

control to eliminate the possibility of chaotic system behaviour. The existence of quasiperiodic oscillations as well as fractional resonances was predicted theoretically [9]. By applying nonlinear analysis methods to data obtained by numerical simulations it was found that the chaotic behaviour may occur via a cascade of period doubling bifurcations [3].

Dynamic AFM may also be understood as a vibro-impacting system where the repulsive tip-sample interaction can be modelled in the most simple case as an instantaneous velocity reflection at a hard wall. Impact oscillators exhibit a complicated dynamic behaviour in the case of grazing impacts, i.e. for collisions with approximately zero velocity. Period-adding bifurcations due to grazing bifurcations were described for a cantilever that is excited at driving frequencies significantly smaller than the free resonant frequency [10, 11]. Grazing bifurcations may also occur in vibro-impact systems that are driven close to the ‘resonance’ of the nonlinear system [12]. Grazing impact events occur in amplitude modulation AFM at the transition from the attractive to the repulsive state. Recently, Hu and Raman demonstrated that such a transition can coincide with a transition from a period-1 to a chaotic state [13].

In addition to the repulsive interaction of the mechanical contact between tip and sample, attractive forces due to van der Waals interaction and capillary forces play an important role. Assuming a Lennard-Jones potential for the tip-sample interaction the dynamics of the forced system was investigated. Period doubling sequences were found for both types of effective tip-sample potential: asymmetric single well and asymmetric double well potential. However, the tip can also escape the double well potential, which gives rise to unpredictable cross-well dynamics in that case [5]. Patil and Dharmadhikari experimentally demonstrated period doubling bifurcations in large amplitude dynamic AFM. They suggest to exploit these bifurcations to achieve a small signal amplification by parametric resonance in non-contact AFM [14]. A period doubling route into chaos was found in AFM where the microscope was operated in contact mode while elastic waves were coupled into the specimen by an ultrasonic transducer [15].

Another important feature of the nonlinear dynamics is the distortion of the nearly sinusoidal tip motion by higher harmonics generation. The occurrence of higher harmonic and subharmonic signal components in the temporal evolution was analysed numerically employing a multiple-degree-of-freedom (MDOF) model. It was demonstrated that the tip motion remains periodic for typical imaging conditions. However, at small tip-sample separations, as are relevant for nanomanipulation, the tip motion becomes unpredictable [16]. Harmonic balance provides an alternative numerical method to compute the steady-state time domain response of a nonlinear system. One advantage of this approach is that the required computational time is independent of time constants and fundamental frequency of the system under investigation. The analysis of the energy dissipation in the tip-sample contact together with the combination of harmonic balance and energy balance equations allows one to estimate model parameters from experimental data and to predict the system response in tapping mode AFM [4]. Since the tip motion is dominantly periodic under most imaging conditions it is also possible to

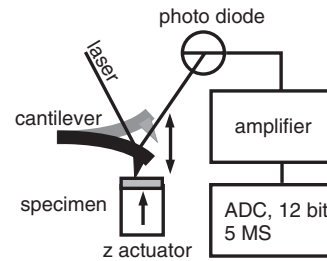


**Figure 1.** Experimental configuration. The cantilever was driven at the fundamental resonance frequency while the sample was slowly moved upwards.

reconstruct the transient forces that act on the force sensing tip in dynamic AFM with methods based on linear system theory [17]. However, as stated before, in close proximity to the specimen surface a complicated dynamics can occur which requires specialized time-series analysis.

In the following, we analyse experimental data with tools of nonlinear dynamics in order to investigate the complex dynamics of the tip-sample interaction at small average tip-sample gaps. We provide experimental evidence for a chaotic behaviour in tapping mode AFM. The experiment is conducted as a so-called dynamic force spectroscopy experiment where the sample is slowly approached towards the tip. In contrast to experiments where the driving amplitude is used as a control parameter, this variation of the sample position corresponds to a typical situation in imaging and nanomanipulation where the amplitude ratio is used as a control parameter.

## 2. Experimental details

A Multimode AFM operated with a Nanoscope IIIa controller (Veeco, Santa Barbara, CA) was equipped with external amplification of the deflection signal (SR560, Stanford Research, Sunnyvale, CA) as illustrated in figure 1. Data were recorded at  $5 \text{ MS s}^{-1}$  (NI PCI-6110, National Instruments, Austin, TX). The microscope was operated in tapping mode with a free oscillation amplitude of approximately  $A_0 = 42 \text{ nm}$ . A v-shaped Si-cantilever was used ( $200 \mu\text{m}$  length; type NSCH 11, nominal spring constant  $4 \text{ N m}^{-1}$ , measured spring constant  $3.8 \text{ N m}^{-1}$ , Silicon-MDT, Moscow; now available from MicroMash, Talinn, Estonia). The cantilever is excited at the fundamental resonance  $f_0 = 46.2 \text{ kHz}$ . The second flexural oscillation mode of the cantilever has its resonance at  $5.346 f_0$ . A silicon (100) wafer with natural oxide layer was cleaned with ethanol and ultra-pure water. For more details and a linear data analysis see [17].

## 3. Data analysis

The raw data are represented in figure 2 after being reduced by a factor of 50. The deflection is shown in arbitrary units as it varies with time (given in sample number) upon the approach to the surface. With increasing sample number the sample is moved upwards thus reducing the average tip-sample distance. Thus, the control parameter of the system is the sample position which is proportional to the sample number. This sample movement approximately corresponds to a set-point

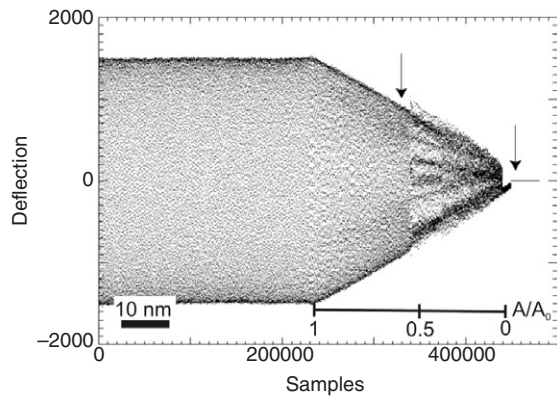


**Figure 2.** Decimated raw data of the photo diode signal versus sample (decimation factor: 50). The amplitude reduction due to the approaching sample and the discontinuity due to the transition between the attractive and the repulsive regime are evident. The arrows indicate the region of the close up shown in figure 4. The scale bar corresponds to the  $z$ -piezo motion. As a guide for the eye a scale bar for the amplitude ratio  $A/A_0$  is also displayed. Due to the bistability, values close to  $A/A_0 \approx 0.5$  may occur twice.

ratio  $A_s$  which is reduced during the experiment starting from  $A_s = 1$  to 0. Since the amplitude ratio  $A/A_0$  is not linear due to the bistability and the offset of the sample position is arbitrary we continue to use the sample number to indicate the sample position in the following. The period of the driving force is  $T = 108.225$ , corresponding to 46.2 kHz. For convenience data were resampled with a delay of  $T = 108.225$  using a fourth-order scheme for interpolation. Thus, the resampling time exactly coincides with the period of the driving force and thus gives a stroboscopic view of the data visualizing the long term variation of the data. Care was taken to comply with the original bandwidth limitations.

The dataset at hand has been analysed using methods from complex systems analysis. Bifurcation analysis has been performed in order to get a coarse classification of the nonlinear modes present in the data. By choosing the period of the external driving force as the inherent timescale of the system the data have been embedded in an artificial phase space via delay coordinates. In this phase space recurrence plots and fractal dimensions have been calculated which can be used for the analysis of the dynamics of the system. By using a windowing technique statistical measures can be applied to the data which give an interesting characterization depending on the operating condition (i.e. on the cantilever rest position). The Kullback–Leibler distance between two statistical distributions was computed for different time windows resulting in a recurrence plot which shows the statistical dependence of the data for various times. Also the mutual information and the cross-correlation of the data give decompositions of the signal according to different periodicities.

### 3.1. Spectrogram

As a first step, the evolution of the spectrum with decreasing average tip–sample distance is shown in figure 3. For orientation, the normalized amplitude of the signal  $A/A_0$  is added. The colours encode on a logarithmic scale for the

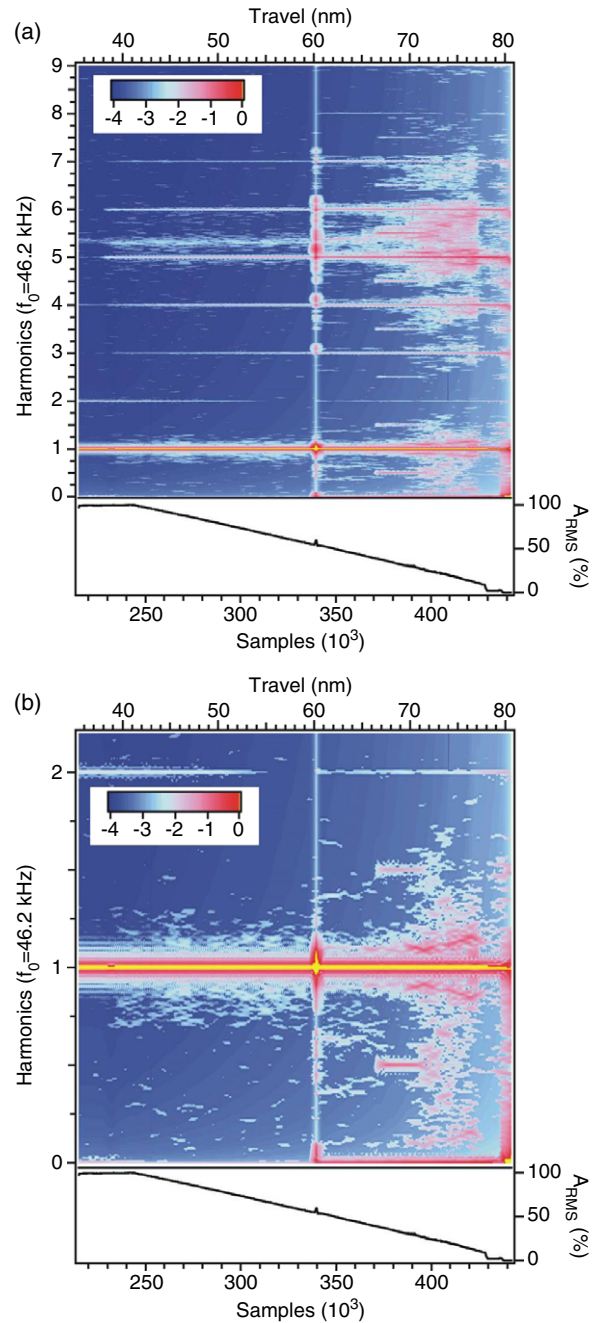


**Figure 3.** Spectrogram of the signal, (a) for a larger frequency range and (b) for a frequency range around the excitation frequency. The spectrum is evolving with increasing piezo-travel (i.e. the average tip–sample distance reduces, sample surface on the right). Close to the surface additional subharmonics occur. In the image, the relative amplitude with respect to the amplitude at the excitation frequency at the given distance is shown. The scale is logarithmic, and only contributions above three times the noise floor are considered. For orientation, the RMS amplitude of the signal normalized to the free oscillation is shown below.

relative contribution of the signal at the frequency of interest with respect to the amplitude at the excitation frequency. Only those contributions appear where the signal is above three times the noise level estimated for the free oscillation. Smaller values are set to the noise level estimate. As the

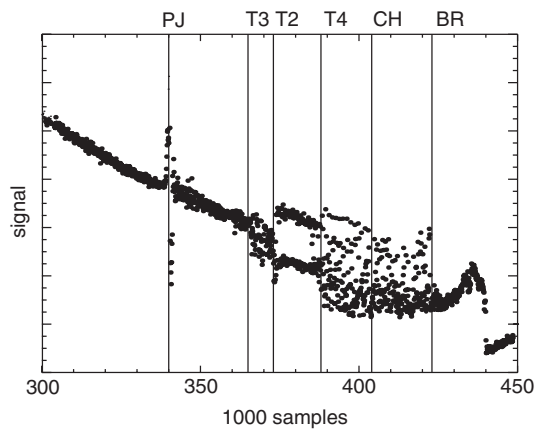


**Figure 4.** Bifurcation diagram of the region of the data between sampling number 300 000 and 450 000.

cantilever approaches the surface, the attractive interaction forces give rise to the excitation of higher harmonics, grouped around the modal frequencies. On further approaching, the higher harmonics generation becomes more pronounced, reaching significant contributions ( $>10\%$  of the amplitude at the excitation). Beyond the onset of repulsive interaction at around 340 kSample, subharmonic regimes are identified well above the noise limit. The spectral behaviour was already analysed earlier [17] and is only repeated for completeness.

### 3.2. Bifurcation diagram

In order to get a coarse overview over the dataset a bifurcation analysis has been performed. In figure 4 a section of the data is shown starting at the moment of first interaction with the surface and ending with the complete contact of the tip at the rest position with the surface. For example, a periodic signal with the period of the driving force would lead to a constant while a subharmonic mode of length  $N$  times  $T$  a periodic resampled signal would result in a structure of length  $N$ .

The bifurcation diagram starts at point (ST), which corresponds to a position where the tip already interacts with the surface. For increasing sample number the tip further approaches the surface until the attractive interaction changes into a repulsive interaction. The transition is indicated by a phase jump (PJ) of the signal. The repulsive regime is then modified to a period-3 behaviour (T3) where three different values of the amplitudes alternate. A further change results in a period-2 state at (T2) where two distinct values of the amplitude can be identified. This regime is quite stable with respect to a change in the tip-sample distance but finally the dynamics of the system transits to a very irregular mode where no structure in the bifurcation diagram can be identified (CH). One can speculate about a period-4 mode which appears directly after the transition from the period-2 mode but the data are not very significant (T4).

The system shows characteristics of a low-dimensional dynamical system with complex periodic and even chaotic behaviour and it is well justified to apply methods from the analysis of dynamical systems such as embedding in delay coordinate spaces and fractal dimensions to the system. It shows several periodic regimes (period-2, -3, -4) as well as a

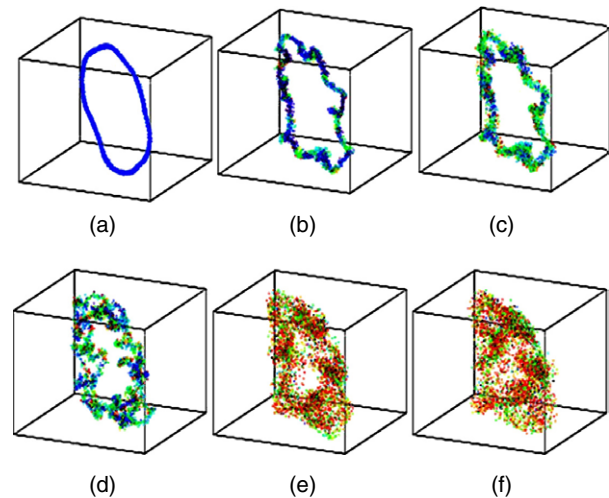


**Figure 5.** 3D phase space embeddings of the deflection data using a delay time of  $T/2$  and  $T/4$ . The colours reflect the local correlation dimension  $D_2$  where blue indicates values near one while red indicates values near two. The panels correspond to the attractive regime (a), the repulsive regime (b), period-3 (c), period-2 (d), period-4 (e) and finally chaos (f) of the system.

chaotic mode. A period-3 behaviour is also a strong indication for the occurrence of chaos [18] and can be approved in the behaviour of the system (CH). Thus, it is reasonable to search for a description of the system using a set of nonlinear coupled ordinary differential equations, which are derived from the most dominant eigenmodes of the continuous system.

### 3.3. Return coordinates

By using integer fractions of the system period an artificial state space can be constructed in which the data can be embedded in order to analyse nonlinear correlations. For a description of the method see [19–22]. In figure 5 the delay coordinate embedding of the time series is shown for six different subregions of the entire dataset using  $T/4$  and  $T/2$  as delays. A window of 4000 samples was used which corresponds to about 40 periods of the driving force. The delay coordinate embeddings were performed just before the times (PJ), (T3), (T2), (T4), (CH) and (BR); thus they correspond to the attractive regime (a), the repulsive regime (b), period-3 (c), period-2 (d), period-4 (e), and finally the chaotic (f) regime of the system.

The return plots can be interpreted as follows. Far away from the surface the tip is in a quasi-free state of motion which is reflected by an almost perfect circular orbit in state space. During the approach of the tip to the surface the perfect orbit becomes more and more distorted until the attractive state (a) becomes unstable and the system transits into the repulsive state which is accompanied by a phase jump (b). After further approach the trajectory shows a period tripling (c), period doubling (d) and after a period quadrupling (e) finally a transition into a fully chaotic motion (f). The chaotic regime is interrupted by regions of quasi-regular behaviour. A particular difficulty inherently in the data is that the data have been recorded in one sweep; therefore, it is not guaranteed that the system is in a stationary state for each regime. In order to

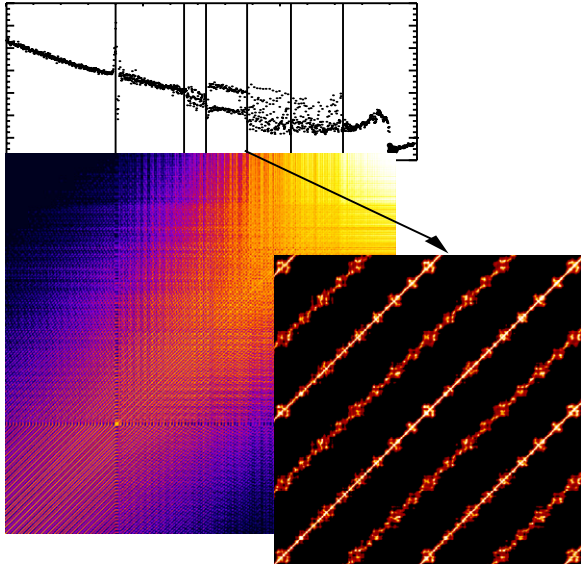


**Figure 6.** Recurrence plot together with the bifurcation diagram, which gives the sample number scale. Distances are colour coded from bright (small distances) to dark (large distances). Furthermore, a close-up of the recurrence plot showing unstable periodic orbits is shown.

check the stationarity of the system a recurrence plot can be helpful.

### 3.4. Recurrence plots

A recurrence plot is a measure for the similarity of different parts of the data. When the dataset has length  $N$  then the recurrence plot is a matrix of size  $N \times N$  where at each position  $i, j$  in the matrix the distance of the data points at position  $i$  and  $j$  is denoted. The distance function can be derived from the absolute value of the data amplitude or can also be a more complex distance in a higher dimensional embedding space. However, for periodic data the recurrence plot results in lines parallel to the diagonal where the distance of the prominent lines to the diagonal of the matrix is given by the period of the dataset. For non-stationary data complex structures emerge along the diagonal of the matrix where the size of the structures perpendicular to the diagonal give a measure for the transition timescale of the non-stationarity. Recurrence plots can also help with the identification of structures in a time series in a qualitative way. These structures can be of intermittent nature, the appearance of an unstable periodic orbit or non-stationarity. Here we define a recurrence plot as the function

$$R(i, j) = \|\vec{x}(i) - \vec{x}(j)\|,$$

where  $\vec{x}(i) \in \mathbf{R}^m$  is the delay coordinate vector of dimension  $m$  (see figure 6).

As can be seen in the recurrence plot, the several periodic and chaotic regimes can be regarded as quasi-stationary. The attractive and repulsive regimes (ST) until (T3) show a nice periodicity coinciding with the periodicity of the driving force. A big difference however appears in the period-3, -2 and -4 regimes. Here additional structures appear along the diagonal with very distinct shapes that appear in a certain succession.

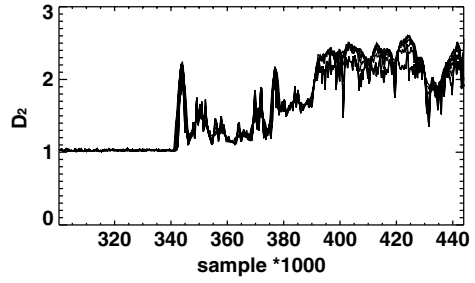


**Figure 7.** Correlation dimension versus sample number computed for different time windows  $N$ . The closest surface approach is located on the rightmost end. At moderate amplitude ratios  $A/A_0$  the motion is periodic as indicated by a correlation dimension value near one. This is typical for an undisturbed line-like (circular) trajectory in phase space which was also observed in the phase space embedding plots. Closer to the surface the trajectory becomes more disturbed, which is reflected by  $D_2$  values up to two, and finally the phase space is more densely filled with trajectory points on a toroidal geometry which is indicated by a  $D_2$  value between two and three.

These structures are due to the temporary vicinity of the trajectory close to an unstable periodic orbit (UPO). Unstable periodic orbits can be viewed as the building blocks of a strange attractor. A chaotic orbit is like a random walk from one UPO to the next. In the period-2, -3 and -4 regimes a periodic sequence of these UPOs appears which corresponds to the periodicity of the regime. In the chaotic regime (CH) the sequence becomes more and more random until no clear periodicity can be found any longer. By identifying the different kinds of UPOs it should be possible to reconstruct the strange attractor.

### 3.5. Fractal dimensions

Another way to characterize the complexity of a dataset is to compute the fractal dimension of the delay-embedded dataset. The larger the fractal dimension the more irregular is the time series. Here, we use the correlation dimension as a measure for the dimensionality of the embedded trajectories. The correlation dimension has a value of one for line-like structures a value of two for surface-like structures and a value of three for space filling, i.e., random structures in a three dimensional embedding space. It is a measure for the degree of freedom that a dynamical system can access. The fractal dimension  $D_2$  can be written as

$$D_2 = d_{\text{corr}} = \lim_{\varepsilon, \varepsilon' \rightarrow 0} \frac{\log C(\varepsilon) - \log C(\varepsilon')}{\log \varepsilon - \log \varepsilon'},$$

where  $C(\varepsilon)$  is the correlation sum given by

$$C(\varepsilon) = \lim_{n \rightarrow \infty} \frac{1}{N^2} \sum_{\substack{i, j=1 \\ i \neq j}}^{\infty} \Theta(\varepsilon - \|\vec{x}(i) - \vec{x}(j)\|).$$

Herein,  $\Theta$  is the Heaviside function.

In figure 7 data are shown using an embedding into a three-dimensional state space. The correlation dimension  $D_2$  is calculated over time in sliding windows with a centre to centre distance of 540 samples ( $\sim 5$  periods of the driving force). The diagram shows the  $D_2$  estimator for several window sizes

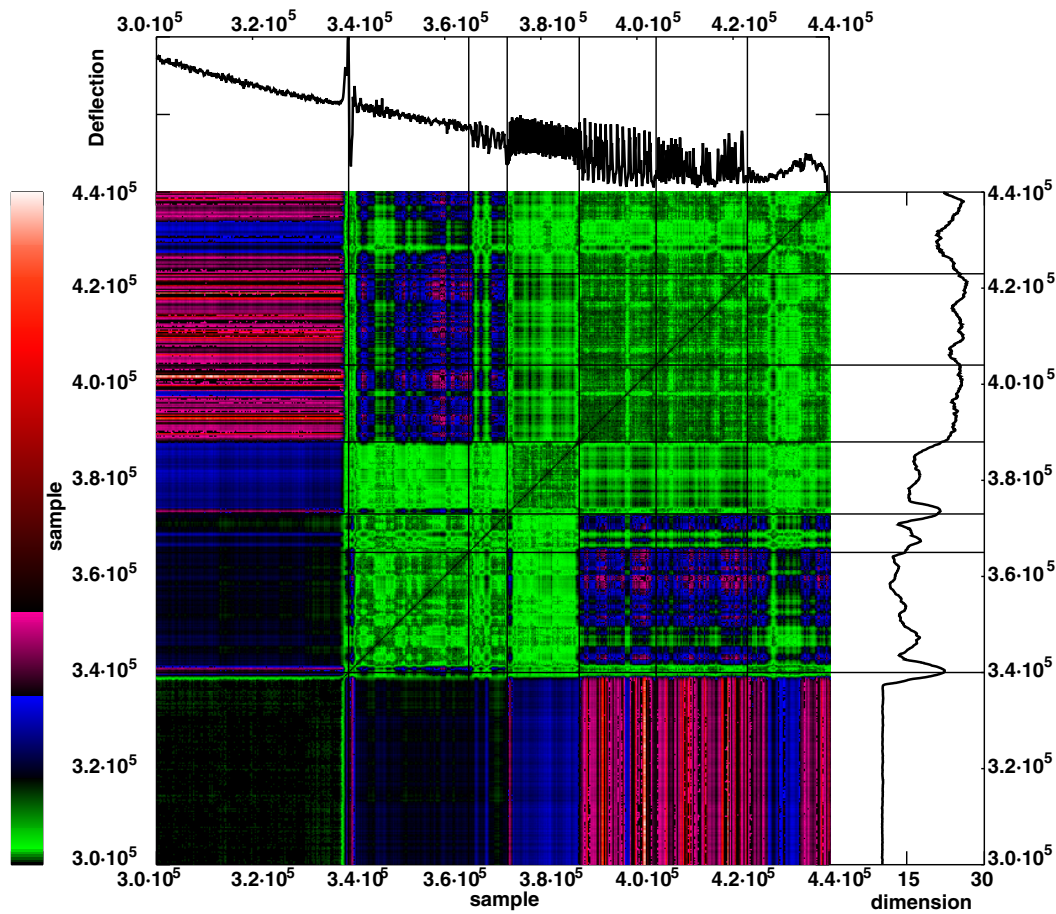


**Figure 8.** Kullback–Leibler distance of the local distributions of the scaling index for different times shown in a recurrence plot style. For comparison the bifurcation diagram and the correlation dimension are added.

ranging from  $N = 540$  to 3240 (30 periods). The smaller the window size the more structure is revealed in time. The overall characteristics do not change significantly in this range. For statistical reasons and to fulfil approximately stationarity conditions a window size of  $N \approx 2000$  is appropriate. The mean of the local dimensions over the dataset gives the correlation dimension  $D_2$ .

One can clearly see that  $D_2$  is of the order of one in the regular regime and then undergoes a transition to higher values in the repulsive regime reflecting the fuzziness of the embedded data. The values of  $D_2$  further oscillate and finally reach values larger than two in the chaotic regime. The  $D_2$ -dimension can thus help in the discrimination between chaotic and regular regimes.

### 3.6. Kullback–Leibler distance

While the correlation dimension as it is used above serves as a time-dependent measure, one is also interested in the relation of the time series to itself at different times and time delays. Therefore, distance measures that quantify the similarity of two fragments of the time series are required. These distance measures can be sensitive to linear dependences, such as the cross-correlation of two random variables, or to general dependences such as the mutual entropy or the Kullback–

Leibler entropy. In the following we focus on the Kullback–Leibler distance, highlighting the diversity of the time series.

Let  $p(i)$  be the frequency distribution of a certain random variable and  $q(i)$  the distribution of another; then the Kullback–Leibler distance of these two distributions is defined as

$$KL = \sum_i p_i \log \frac{p_i}{q_i}.$$

The Kullback–Leibler distance is a measure for the diversity of two statistical distributions and is measured in bits. In figure 8 the Kullback–Leibler distance of every distribution of the so-called local scaling index with every other in the windowed dataset is shown. The distribution of scaling indices [23] is a realization of the distribution of point-wise dimensions and is closely related to the fractal dimension of point distributions based on delay coordinate embeddings of time series. The plot can be seen as recurrence plot of the scaling index distributions revealing the properties of the attractor in state space. Black means a small distance while green, blue and red mean increasing distance. Obviously the recurrence plot can be separated into two regions: a dark green region at the lower left and a bigger lighter green region upper right, which itself shows a rich substructure. The green colours mean that the data in this region are very similar and clearly reflect the overall classification of the time series in the various periodic

and chaotic regimes. The Kullback–Leibler distance can thus be used as a measure for the deviation of the behaviour of the tip to a nominal state without knowing the system parameters. As long as the Kullback–Leibler distance to the initial (free) state is small the system is in the regular regime. A jump in the Kullback–Leibler distance shows a transition in the behaviour of the dynamic system.

### 3.7. Period analysis

One interesting question is about the length of the periodic orbit. For the undisturbed system this length is just the period of the driving force but for the interacting system this period can become longer and in the chaotic regime this period length approaches infinity. In order to obtain a measure for the length of the period one can use a correlation measure which, in the simplest case, is the autocorrelation function for different delay times. It is also possible to use generalized measures for the dependence of the time series with a time shifted copy of itself, similar to the mutual information. It is closely related to the Kullback–Leibler distance and gives the information that can be learned from one system while knowing the information from the other system. It is measured in bits and is invariant under a remapping of the two distributions.

For a joint probability distribution  $p(i, j)$  the mutual information is defined by

$$M = \sum_{ij} p_{ij} \log \frac{p_{ij}}{p_i p_j}.$$

It can be interpreted as the information about the joint system minus the information about the single independent systems. For a comprehensive discussion see [24, 25]. The mutual information can now be used as a correlation measure of the time series with a shifted copy of itself. In figure 9 the linear correlation coefficient and the mutual information are shown for different regimes of the system. The black curve denotes time delay  $T$ , while the red curve denotes  $3T$ , the blue curve denotes  $2T$  and the green curve denotes  $T/2$ .

One can clearly see that far away from the surface the period of the driving force dominates over all other periods, but after approaching the surface the strongest mode is first  $3T$  then  $T$  and the  $2T$ , which reflects a different time coherence of the system. In the chaotic regime the linear and the nonlinear correlation decrease strongly indicating the loss of memory of the system for chaotic behaviour.

## 4. Conclusions

The system under consideration shows features that are typical for a dynamical system with a low number of degrees of freedom in the regular and chaotic regime. At large tip–sample gaps the system is in a regular regime. During the approach in a dynamic force spectroscopy experiment a phase jump, a period-3, period-2 and a period-4 regime developed and were followed by a chaotic regime. This leads to limitations in typical dynamic AFM experiments where the system response is only measured in a narrow frequency band around the driving frequency. In applications such as imaging, nanomanipulation or dynamic force spectroscopy, only a small part of the dynamic response is used for feedback. In the case of a complicated system response thus systematic errors or

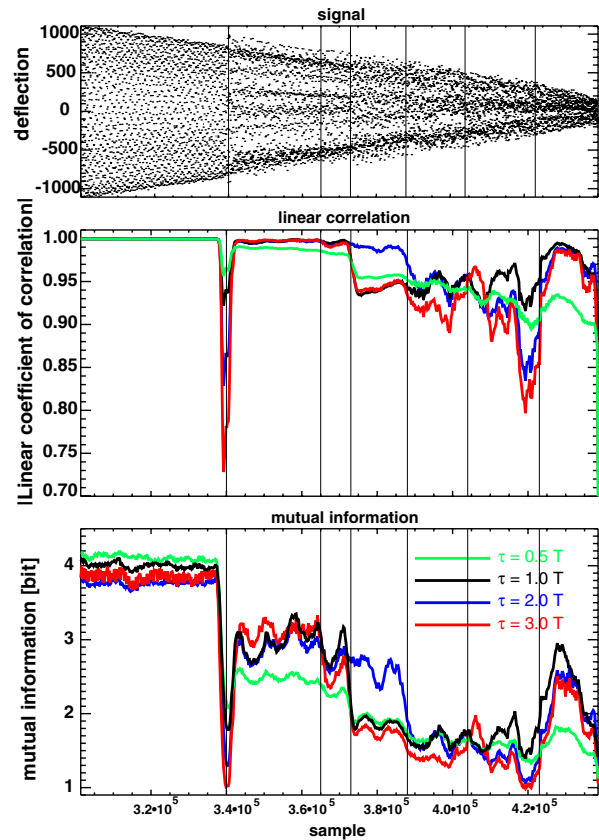


**Figure 9.** Deflection signal, linear correlation coefficient and mutual information versus tip–sample distance (sample number). In the lower two panels are shown the correlation measures for different time delays. The black curve denotes time delay  $T$  ( $= 108.25$ ), while the red curve denotes  $3T$ , the blue curve denotes  $2T$  and the green curve denotes  $T/2$ . The overall tendency is similar in both correlation measures. In some regions, however, the mutual information reveals more details and an enhanced contrast between the different time delays.

(This figure is in colour only in the electronic version)

noise can corrupt the measured surface profile or interaction force.

Comparable system characteristics have been observed for the Duffing oscillator [21], which can serve as a model system for an AFM operated at a small average tip–sample gap. In the case of a chaotic signal the usual measures (frequency shift or the amplitude) become meaningless and can no longer be used as characteristic values that describe the state of the system and the physical properties of the underlying surface. In this case the fractal dimensions and entropies become a meaningful alternative. As the nonlinear characteristics of the system crucially depend on the physical properties of the underlying sample these measures (correlation dimension, mutual information) express the physical parameters of the system. For a remapping from the dimensions and entropies, however, one needs a numerical or analytical model for the physics of the system.

## Acknowledgments

This work was supported by the German Federal Ministry of Education and Research BMBF under Grant No. 03N8706. We gratefully acknowledge the generous support by R Guck-

enberger, Max-Planck-Institut für Biochemie, Martinsried, Germany.

## References

- [1] García R and Pérez R 2002 Dynamic atomic force microscopy methods *Surf. Sci. Rep.* **47** 197–301
- [2] Hunt J P and Sarid D 1998 Kinetics of lossy grazing impact oscillators *Appl. Phys. Lett.* **72** 2969–71
- [3] Basso M, Giarré L, Dahleh M and Mezić I 2000 Complex dynamics in a harmonically excited Lennard-Jones oscillator: microcantilever–sample interaction in scanning probe microscopes *J. Dyn. Syst. Meas. Control* **122** 240–5
- [4] Sebastian A, Salapaka M V, Chen D J and Cleveland J P 2001 Harmonic and power balance tools for tapping-mode atomic force microscope *J. Appl. Phys.* **89** 6473–80
- [5] Rützel S, Lee S I and Raman A 2003 Nonlinear dynamics of atomic-force-microscope probes in Lennard-Jones potentials *Proc. R. Soc. A* **459** 1925–48
- [6] Nony L, Boisgard R and Aimé J P 2001 Stability criterions of an oscillating tip-cantilever system in dynamic force microscopy *Eur. Phys. J. B* **24** 221–9
- [7] Ashhab M, Salapaka M V, Dahleh M and Mezić I 1999 Dynamical analysis and control of microcantilevers *Automatica* **35** 1663–70
- [8] Ashhab M, Salapaka M V, Dahleh M and Mezić I 1999 Melnikov-based dynamical analysis of microcantilevers in scanning probe microscopy *Nonlinear Dyn.* **20** 197–220
- [9] Sasaki N, Tsukada M, Tamura M, Tamura R, Abe K and Sato N 1998 Dynamics of the cantilever in noncontact atomic-force microscopy *Appl. Phys. A* **66** S287–91
- [10] de Weger J, van de Water W and Molenaar J 2000 Grazing impact oscillations *Phys. Rev. E* **62** 2030–41
- [11] van de Water W and Molenaar J 2000 Dynamics of vibrating atomic force microscopy *Nanotechnology* **11** 192–9
- [12] Budd C and Dux F 1994 Intermittency in impact oscillators close to resonance *Nonlinearity* **7** 1191–224
- [13] Hu S and Raman A 2005 Subharmonics and chaos in tapping mode atomic force microscopy *ASME Conf. (Orlando, FL, 2005)* (unpublished)
- [14] Patil S and Dharmadhikari C V 2003 Small signal amplification using parametric resonance in NcAFM imaging *Appl. Surf. Sci.* **21** 7–15
- [15] Burnham N A, Kulik A J, Gremaud G and Briggs G A D 1995 Nanosubharmonics: the dynamics of small nonlinear contacts *Phys. Rev. Lett.* **74** 5092–5
- [16] Stark R W 2004 Spectroscopy of higher harmonics in dynamic atomic force microscopy *Nanotechnology* **15** 347–51
- [17] Stark M, Stark R W, Heckl W M and Guckenberger R 2002 Inverting dynamic force microscopy: from signals to time-resolved interaction forces *Proc. Natl Acad. Sci. USA* **99** 8473–8
- [18] Li T-Y and Yorke J A 1975 Period three implies chaos *Am. Math. Mon.* **82** 985–92
- [19] Takens F 1981 *Detecting Strange Attractors in Turbulence in Dynamical Systems and Turbulence, Warwick 1980 (Springer Lecture Notes in Mathematics vol 898)* (Berlin: Springer) p 366
- [20] Sauer T, Yorke J and Casdagli M 1991 Embedology *J. Stat. Phys.* **65** 579–616
- [21] Battelli F and Palmer K J 1993 Chaos in the Duffing equation *J. Diff. Eqns* **101** 276–301
- [22] Packard N H, Cratchfield J P, Farmer J D and Shaw R S 1980 Geometry from a time series *Phys. Rev. Lett.* **45** 712–6
- [23] Jamitzky F, Stark R W, Bunk W, Thalhammer S, Rätz C, Aschenbrenner T, Morfill G E and Heckl W M 2000 Scaling-index method as an image processing tool in scanning-probe microscopy *Ultramicroscopy* **86** 241–6
- [24] Shannon C E 1948 A mathematical theory of communication *Bell Syst. Tech. J.* **27** 379  
Shannon C E 1948 A mathematical theory of communication *Bell Syst. Tech. J.* **27** 673
- [25] Fraser A M and Swinney H L 1986 Independent coordinates for strange attractors from mutual information *Phys. Rev. A* **33** 1134